

Received January 6, 2019, accepted January 29, 2019, date of publication February 1, 2019, date of current version February 20, 2019.

Digital Object Identifier 10.1109/ACCESS.2019.2897092

Wideband High Gain Printed Quasi-Yagi Diffraction Gratings-Based Antenna for 5G Applications

ESSA H. MUJAMMAMI^{ID}, (Graduate Student Member, IEEE),

AND ABDELRAZIK B. SEBAK^{ID}, (Life Fellow, IEEE)

Electrical and Computer Engineering Department, Concordia University, Montreal, QC H4B 1R6, Canada

Corresponding author: Essa H. Mujammami (e_muja@encs.concordia.ca)

ABSTRACT A broadband high-gain printed Quasi-Yagi antenna with a perturbation-based planar dielectric lens is presented. The perturbation design parameters are based on the diffraction gratings theory for gain enhancement, radiation pattern improvement, and higher order modes suppression. The proposed antenna provides 94.5 % aperture efficiency with a high gain of 15 dBi at 30 GHz, high radiation efficiency of $\sim 90\%$, and (24–40) GHz ultra-wide matching ($S_{11} < -10$ dB) bandwidth. The measured cross-polarization is lower than -20 dB in both E - and H - planes. With these features in addition to being low-profile and lightweight, this antenna is suitable for various millimeter-wave applications.

INDEX TERMS 5G antenna, high gain, lens, diffraction gratings, Quasi-Yagi.

I. INTRODUCTION

Millimeter waves (mmWaves) open up more spectrum allocations for the 5G wireless networks that will feature native support for new kinds of network deployments, including ultra-dense radio networking with self-backhauling, lower outage probability, much higher bit rates, more efficient spectrum reuse, and mesh-like connectivity. All these features make mmWaves an excellent candidate solution for future 5G wireless networks. Achieving these prodigious advantages requires new power-efficient air-interface standards, robust statistical spatial channel modeling, more advanced high gain antennas, and streamlined beamforming algorithms among many other design challenges [1]. Designing a mmWave antenna for 5G system is a crucial issue since it should meet some challenging requirements. First, the operating bandwidth should be sufficiently wide for reasonable data rate [2]. Second, the antenna system's gain should be high to compensate for the path losses of the mmWave propagation. Third, the compatibility with standard planar low-cost processing techniques for mmWave monolithic integrated circuit (MMIC) and high volume production [3].

Quasi-Yagi antenna and dielectric lens antenna (DLA) are among the recently developed mmWave antennas. For

advantages of low profile, lightweight, ease of fabrication and installation, high directivity, high radiation efficiency etc, Quasi-Yagi antenna has attracted much attention for use in the microwave and mmWave applications [4], [5]. The bandwidth performance of the Quasi-Yagi antenna is highly reliant on its feeding network. Consequently, different excitation and transition methods have been proposed in the literature to achieve broadband. A microstrip line-to-coplanar strip line (MS-to-CPS) transition is proposed in [6]. This excitation method results in about 30.3% fractional bandwidth (FBW). Using coplanar waveguide-to-coplanar-strip (CPW-to-CPS) transition, 11.6%–44% FBW can be achieved as reported in [7] and [8]. Coplanar stripline-to-slotline (CPS-to-SL) is used in [9] and [10] providing FBW of 52.6% and 97%, respectively. A Quasi-Yagi antenna with 83.7% FBW is reported in [11] using a microstrip-to-slot line transition (MS-to-SL) structure. CPS-to-SL and MS-to-SL have the maximum FBW between these techniques. MS-fed [12], and CPW-fed [13] are also used for exciting the Quasi-Yagi antenna with a broadband. The printed Quasi-Yagi antenna has been used as endfire antenna in different frequency bands for diverse applications. In [14] a Quasi-Yagi antenna is proposed for WiMAX and WLAN applications. The antenna achieves two wide bandwidths, 2.3–3.7 GHz (46.7%) and 5–6.25 GHz (22.2%), and high stable gain (8.5 ± 0.9 and 9 ± 1 dB) within these two operation

The associate editor coordinating the review of this manuscript and approving it for publication was Chow-Yen-Desmond Sim.

bands. However, the antenna structure is bulky and difficult to be integrated with planar structures. A printed Yagi-antenna with bandwidth of (1.84-4.59) GHz and gain (4.5-9.3) dBi for WLAN, WCDMA, LTE applications is presented in [15]. Nevertheless, there is a large variation in the antenna gain over the reported bandwidth. The author suggests decreasing the number of the directors to retain gain stability. However, this will reduce the total gain. Another Quasi-Yagi antenna that is demonstrated in [16]. The design, simply, integrates an arc-shaped strip, which serves as a near-field resonant parasitic (NFRP) element, and a coplanar-waveguide (CPW)-fed semiloop antenna. The antenna has a very compact electrical size of $0.17\lambda_0 \times 0.43\lambda_0$ and 5.6 dBi directivity. However, this Quasi-Yagi antenna has a narrow bandwidth of (5.06%) FBW and does not meet the requirements of 5G antenna system. A microstrip-fed millimeter-wave Yagi-Uda antenna with applications as a single element radiator or for switched-beam systems with gain (10 dB) is presented in [17]. The antenna has a wideband operation (22–25 GHz). Although 1×2 antenna array of this Yagi-Uda has (9-13) dBi gain, still insufficient for 5G communication link [1], [3]. In addition, the antenna electrical size of $2.3 \lambda_0 \times 3.3 \lambda_0$ is relatively large. In [18], a 60-GHz 1×4 antenna array with ladder-like multi-directors is presented. The single-stage multi-directors are introduced for gain improvement, side lobes reduction, and bandwidth extension. The antenna exhibits a medium gain of 11 dBi. Such gain does not meet the minimum 5G system gain requirement [1], [3]. On the other hand, DLAs are widely used for gain enhancement purpose, but the DLAs of high gain are, mostly, designed with thick substrates or bulky structures. A patch fed planar dielectric slab waveguide extended hemi elliptical lens antenna is described in [19]. The lens weighs only 90 g. The maximum lens dimensions are $11\lambda \times 13\lambda$ in the lens plane and it is 0.6λ thick. The operational bandwidth is 18 to 30 GHz with 18.5 dB measured gain at 28.5 GHz. In [20], a 120mm diameter and 6.4mm thick planar Luneburg lens antenna is presented. The lens is composed of a shape contoured fixed dielectric constant disc, with a total weight of 45 g with 16.8 dB gain, 10% fractional bandwidth (FBW) and cross-polarization better than -20 dB. The size of both antenna systems reported in [19] and [20] is electrically large.

In this paper, we present a new type of planar antenna as a potential candidate for 5G applications. The proposed antenna is a combination between a Quasi-Yagi antenna and a planar dielectric lens. The single element of the proposed antenna has four major advantages over the previously mentioned antennas. A gain improvement of 3.5–5.5 dB compared to the two elements array reported in [17], more efficient in terms of wide bandwidth with more than 17 GHz (40 % FBW), smaller compact size, the same gain of [17] can be obtained with only $0.5\lambda_0 \times 4.8\lambda_0$ including the planar dielectric lens and more importantly, with an excellent gain stability over a broad frequency band. The basic idea of the new antenna relies on controlling the wave propagation characteristics of a thin dielectric slab waveguide (DSW) by

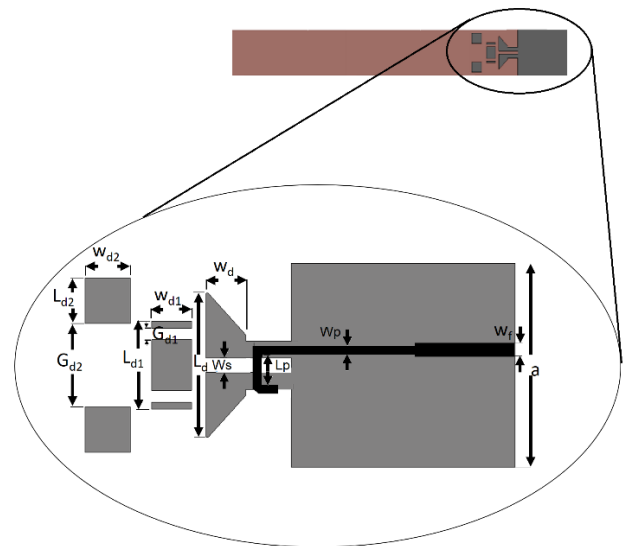


FIGURE 1. Planar Quasi-Yagi antenna with a plain DSW.

introducing a perturbation in the DSW. Although this method has been used previously to improve the performance of different antenna systems and microwave components [21]–[24], however, the provided effective permittivity calculation was reported with via diameter dependency only, while there is another factor that should be accounted in designing this type of planar dielectric lenses, which is the spacing between air-vias. The provided effective permittivity calculation here includes the radius and the spacing between the air holes in two dimensions based on the diffraction gratings and the effective medium theories. Consequently, a design methodology for high gain planar Quasi-Yagi with dielectric lens antenna is presented. The proposed methodology provides more flexibility to the design and fabrication processes.

II. ANTENNA DESIGN CONFIGURATION THEORY AND ANALYSIS

In this work, the analysis and design are based on Rogers 6010 substrate with dielectric constant of 10.2 and loss tangent of 0.0023. The substrate has a thickness of 0.381 mm. Full-wave electromagnetic (EM) simulator CST ver. 16 and HFSS ver. 16. have been adopted for the simulation.

A. ANTENNA DESIGN CONFIGURATION

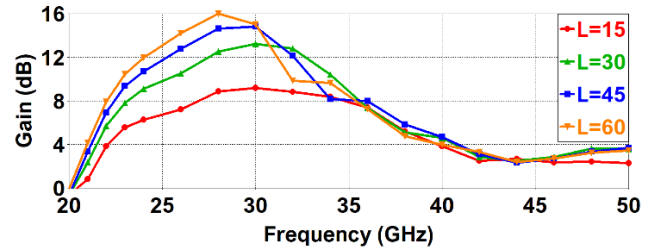
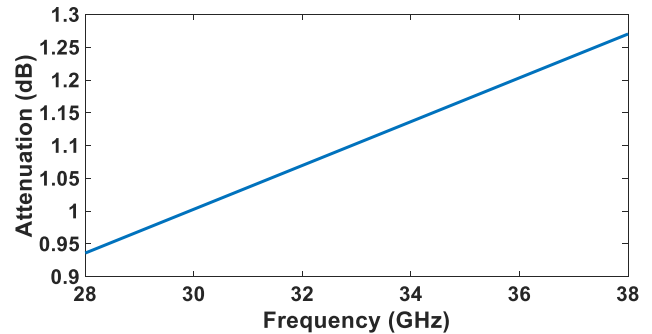
The proposed 28-38 GHz Quasi-Yagi, basically, consists of two major parts as shown in Fig. 1. The first part includes driver dipole, reflector, two-stage directors and, MS-to-SL transition structure and is located on the top layer of the substrate. On the bottom layer, a U-shaped MS-to-SL balun is placed to feed the driver dipole. This part works as an excitation source for the DSW, which is the second part of the antenna. The conventional rectangular driver of the printed Quasi-Yagi antenna has a narrower bandwidth compared to the tapered one, while the tapered driver has a tilted edge

TABLE 1. Dimensions of the proposed antenna.

Parameter	(mm)
a	4.5
b	58.5
w_f	0.235
w_s	0.330
w_p	0.178
w_d	0.924
w_{d1}	0.924
w_{d2}	1.050
w_{rs}	0.150
L_{rs}	2.400
L_d	3.350
L_{d1}	2.050
L_{d2}	1.050
L_p	0.723
G_{d1}	0.260
G_{d2}	1.940
r_h	0.500
d_r	0.254
s_x	0.254
s_z	0.254

with respect to the reflector. Therefore, the driver is tapered to improve the antenna bandwidth performance. The initial length of the driver dipole is selected to be around one effective wavelength (λ_{eff}) of the center of frequency in the desired frequency band, to increase the dipole directivity compared to half-wavelength dipole used in the ordinary Yagi-Uda antenna [25]. Furthermore, the antenna directivity is boosted by two stages of passive multi-directors closely spaced by $0.1 \lambda_{\text{eff}}$ between the first director and the driver and $0.142 \lambda_{\text{eff}}$ between the second stage of directors and the first stage. Another function of multi-directors is providing a good impedance matching for the antenna [18]. The closer spacing between the driver and the first director as well as between the two directors ensures maximum electromagnetic coupling due to space wave and the substrate's surface wave [26]. About $0.25 \lambda_{\text{eff}}$ from the driving dipole, the microstrip ground plane is located and acts as a reflector with $1.34 \lambda_{\text{eff}}$ width. The antenna is designed to have an input impedance of 50Ω and is connected to a microstrip line with $w_f = 0.365\text{mm}$ ($Z_0 = 50 \Omega$) followed by another microstrip line of $w_p = 0.178\text{mm}$ width ($Z_1 = 67 \Omega$). This impedance is selected initially to match the input impedance of the Quasi-Yagi array at the center of the driven element and is usually small. It is strongly influenced by the spacing between the reflector and the driver [25]. The last microstrip line is curved in U-shape to feed the driving dipole through an MS-to-SL transition, providing a single-ended-to-differential conversion with a wide bandwidth. The U-shaped MS-to-SL balun is optimized to achieve a good impedance matching. The directivity of the proposed Quasi-Yagi antenna is enhanced by extending the plain dielectric substrate as a dielectric lens. Table 1 contains the design parameters of the proposed antenna.

Since the desired frequency band is 28-38 GHz, as candidate frequencies for 5G applications [1], the center frequency

**FIGURE 2. Gain over frequency for different plain DSW lengths.****FIGURE 3. Attenuation over frequency for a plain DSW of 50mm length.**

is selected around 34 GHz. Consequently, the antenna's gain stability is expected to vary ± 1 dB around the center frequency. However, simulation results show that the performance of the Quasi-Yagi antenna with a plain DSW lens is, dramatically, degraded as the DSW length increases as shown in Fig. 2. The antenna gain is not achieved as expected and converges to the original gain of the planar Quasi-Yagi antenna without extended DSW lens.

To understand the reason behind the dramatic gain decline, wave propagation characteristics in the extended DSW are investigated. It is well known that attenuation in a lossy dielectric material is the dominating effect of wave propagation. However, the wave attenuation level for all frequencies in the band ranges below (0.93 to 1.27) dB throughout the entire DSW length as shown in Fig. 3, while the gain sharply drops when the frequency exceeds 32 GHz. The investigation is extended to the propagating modes which could be supported by the DSW. It is commonly desired to operate an antenna system with a single mode of propagation, and this can be achieved by respecting the cutoff frequency for a certain mode in a DSW. However, the geometry of the proposed antenna with its rectangular DSW supports TM_{mn} modes. For a thin DSW with a high dielectric constant, the boundary between the surrounding free space (air) and the DSW can be approximated by a perfect magnetic conductor (PMC). Then, 10.44 GHz, 20.87 GHz, and 31.31 GHz are the cutoff frequencies of the three first modes in the plain DSW, consequently, higher order modes (HOM) are expected to propagate with the fundamental TM_{10} mode. Nevertheless, the symmetry of the antenna structure prevents TM_{20} mode from propagation while TM_{30} mode is expected to exist.

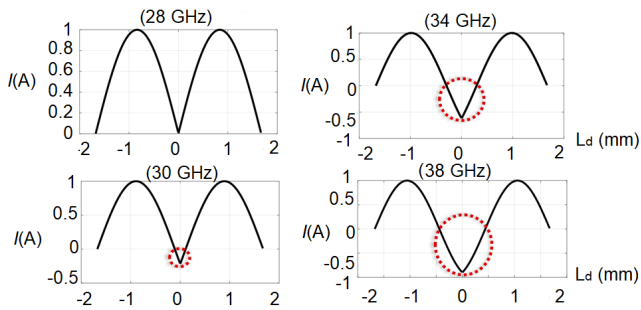


FIGURE 4. Current distribution on a finite length dipole with an opposite current polarity for different frequencies.

Another source of undesired propagating modes is the length of the printed dipole. When the dipole length exceeds one full wavelength, the current distribution on the two sides of the dipole starts to change its polarity [25]. The negative polarity current could excite undesired HOM (TM₃₀) which can be supported by DSW. As the frequency increases, the dipole electrical length increases, therefore, the negative current polarity portion increases accordingly as shown in Fig.4. Some large canceling effects in the radiation pattern would be expected [27]. This could explain the dramatic gain declining in the upper operational band frequencies of the Quasi-Yagi antenna (32-38) GHz. The effect of HOM becomes worst as the length of the extended ordinary DSW increases, where it destructively interferes with the fundamental mode due to the total internal reflection (TIR), as well as, the increase of attenuation with length. It also justifies the shift in the maximum gain to the lower band frequencies which have low attenuation, and mainly, are below the cutoff frequency of TM₃₀HOM.

Since HOMs are undesired for their influence on the antenna performance, they should be suppressed. There are different techniques to avoid their propagation. One way is to limit the operational bandwidth to lower than lowest HOM cutoff frequency to avoid its propagation. In practice, 5% of the HOM cutoff frequency safety margin is usually recommended [28]. Though, this way results in a narrow bandwidth system. Another way is to limit the length of the dipole to one effective wavelength so that HOM excitation through opposite polarity current is prevented. However, this technique reduces the directivity of the finite length dipole and makes the antenna matching so difficult, where the input impedance, in this case, goes to infinity. Another way is perturbing the antenna structure by introducing, for example, rectangular corrugations or holes in the waveguide perpendicular to the propagation direction [29]. In other words, DSW's surface should be shaped to act as diffraction gratings. This implies enforcing new boundary conditions on DSW surface result in varying the surface homogeneity and hence reducing the effective dielectric constant of DSW. This technique implies, also, controlling DSW surface phase condition in a way allows the fundamental mode to propagate and suppress the undesired HOM [30].

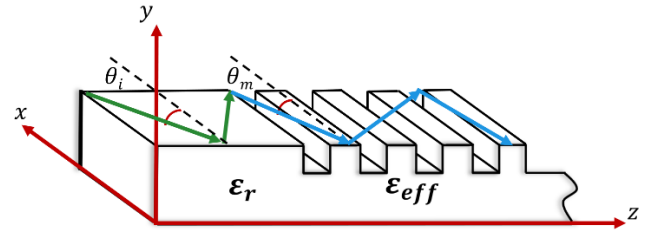


FIGURE 5. DSW Geometry using one dimensional diffraction gratings.

B. POPAGATING MODES ANALYSIS USING DIFFRACTION THEORY

The wave inside an ordinary DSW is a combination of fundamental mode and undesired modes. Therefore, the DSW surface should be modified to block HOM propagation. In fact, diffraction gratings theory provides a solution for such a situation. This is, simply, achieved by introducing grooves to the DSW surface as shown in Fig. 5, then any transmitted wave through or reflected off that surface, is diffracted according to the following grating equation [31]

$$n \sin \theta_m = n_i \sin \theta_i + mG\lambda_0 \tag{1}$$

where G is the groove frequency or groove density, more commonly called “grooves per millimeter”, m is the order of the diffracted mode, n is the refractive index of the medium it will be reflected or transmitted to, n_i is the refractive index of the medium contains the incident wave, θ_m and θ_i are the reflected or transmitted and the incident plane wave angles respectively. λ is the wavelength in the incident region. For a specific wavelength λ, all values of diffraction order m that satisfy |mλ/d| < 2 represent propagating diffraction orders, d = 1/G is the corrugation period in millimeter. The special case m = 0 leads to the law of reflection θ₀ = -θ_i for all λ. The grating, in this case, acts as a mirror, so the wave is reflected. This is called the zero order diffraction mode (ZOD). In fact, ZOD mode is useful for designing planar high gain broadband endfire mmWave antennas. The proposed DSW structure allows the wave propagation as ZOD mode, prevents higher order diffraction modes, and ensures the guidance of the wave along the corrugated DSW structure due to TIR. Another application of ZOD mode is coupling one guided mode to another guided mode in a DSW [30], [31]. The fundamental and HOM are treated as two different incident waves to a diffraction grating surface with different incident angles. Spatially, grating surface modulates the amplitude of the propagating wave through its train of rectangular corrugations. The modulated wave in the spatial domain can be analyzed in the frequency domain for more details about different designing parameters. Since ZOD mode is used here, the corrugation period d can take any fraction value of the wavelength, provided that it should be much smaller than the wavelength (d ≪ λ), commonly named subwavelength grating. The effective dielectric constant of the corrugated DSW depends on the corrugation duty cycles (f) and (f_h), which determine the corrugation width

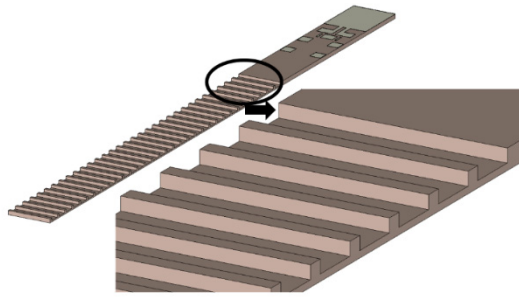


FIGURE 6. PLDC geometry as ruled diffraction gratings.

and depth respectively:

$$\epsilon_{eff} = \epsilon_r + (1 - f)(1 - f_h)(1 - \epsilon_r) \quad (2)$$

To ensure the single mode of propagation, the effective dielectric constant of the grating surface should be designed to allow the fundamental mode to propagate with a real phase constant (β_{10}) while the possible propagating HOMs would have imaginary phase constants ($\beta_{20}, \beta_{30}, \dots$) according to the following equation:

$$\frac{\beta_{n0}}{k} = \sqrt{1 - \left(\frac{n\lambda_0}{2a\sqrt{\epsilon_{eff}}}\right)^2}, \quad n = 1, 2, 3, \dots \quad (3)$$

a is the DSW width.

III. DEVICE DESIGN

A. PARALLEL LINES DIELECTRIC CORRUGATION

Parallel lines Dielectric Corrugation (PLDC) is a corrugation in a dielectric substrate with a corrugation period, width and depth of d , w_c and L_c , respectively. Fig. 6 shows the PLDC geometry, which is, basically a ruled diffraction grating but is used in the endfire direction.

For a high and stable gain with a broadband Quasi-Yagi dielectric lens antenna, free of HOMs, PLDC should be designed according to (2) and (3). The dielectric constant of the corrugated part of DSW is reduced from ϵ_r to ϵ_{eff} . Therefore, the cutoff frequencies of the first three propagating modes are increased, so that TM_{20} and TM_{30} cutoff frequencies become out of the 30-38 GHz band. A schematic illustration for the modes propagation inside the plain and corrugated DSW is shown in Fig. 7. Moreover, the propagation characteristics are highly improved compared to the case of Quasi-Yagi antenna with a plain DSW as shown in Fig. 8a. When the corrugation period is much less than the effective wavelength ($d \ll \lambda_0/\sqrt{\epsilon_{eff}}$) of the maximum frequency in the band (i.e. 38 GHz), the gain is stable, where only the fundamental mode is propagating along the guiding structure to the end of corrugated DSW, providing the expected gain. It can be seen, also, in Fig. 8b that the antenna has a good impedance matching (below -15 dB) for all periods satisfy ($d \ll \lambda_0/\sqrt{\epsilon_{eff}}$), but if the corrugation period becomes a significant fraction of the effective wavelength, then the phase of the incident wave and DSW surface's phase matching condition is not held, HOM starts to propagate and interferes

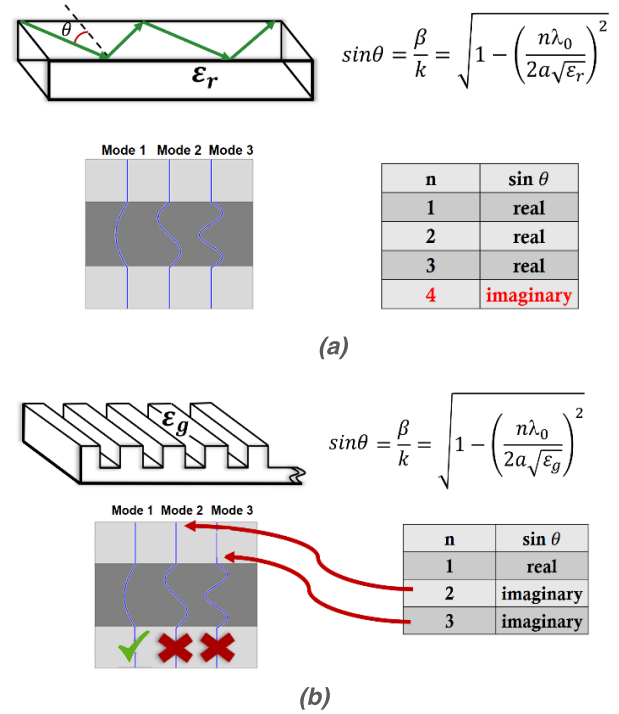


FIGURE 7. Schematic diagram for the modes propagation inside: (a) Plain DSW. (b) Corrugated DSW.

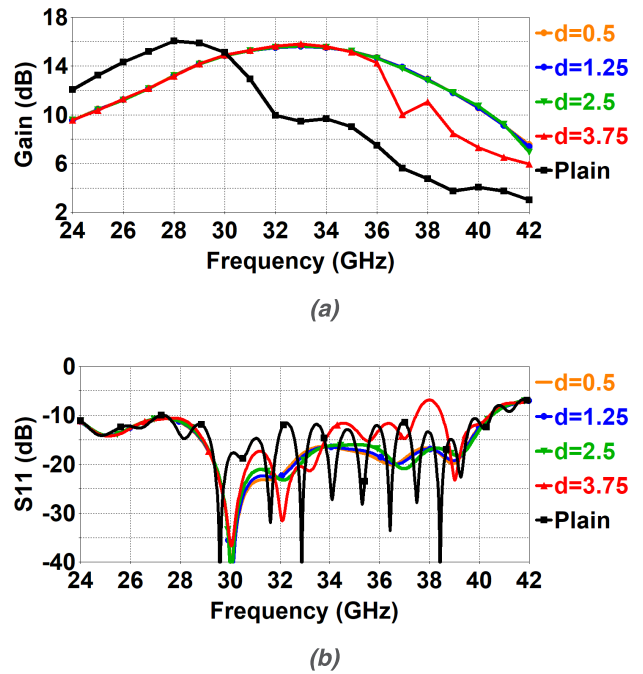


FIGURE 8. PLDC Performance variation with corrugation period: (a) Gain, (b) Return Loss.

the fundamental mode. If the corrugation period reaches $\lambda_0/\sqrt{\epsilon_{eff}}$, the wave is diffracted as $m = -1$ diffracted mode into the surrounding medium with a large portion is reflected to the antenna and the gain will sharply decline.

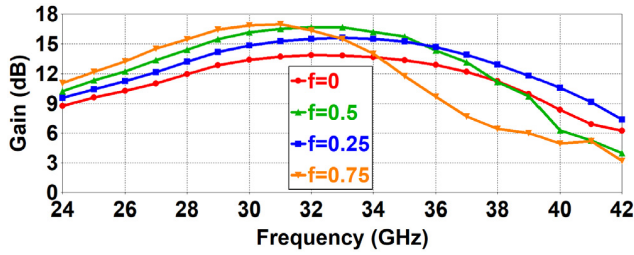


FIGURE 9. PLDC Gain and bandwidth variation with corrugation width.

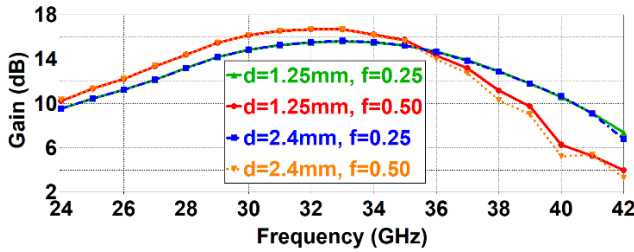


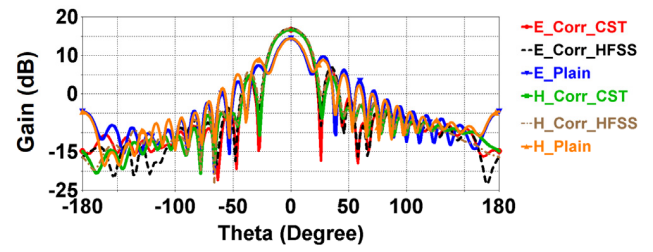
FIGURE 10. PLDC performance dependency on the corrugation Duty Cycle.

The corrugation width and depth control the gain and bandwidth of PLDC lens antenna. Considering that corrugating in DSW is a sort of spatial modulation, it is well known that a rectangular corrugation in the spatial domain is a sinc function in the frequency domain. When the corrugation cross-section area ($w_c \cdot L_c$) increases, consequently the gain increases. On the other hand, the frequency bandwidth is inversely proportional to corrugation width w_c , analogous to a wide or narrow duration time domain pulse. So w_c should be optimized for maximum gain and frequency bandwidth. Fig.9 depicts the gain and bandwidth variation with corrugation width. $w_c = 0$ means zero width corrugation, the thickness of the entire corrugated DSW is reduced to $(h-L_c)$.

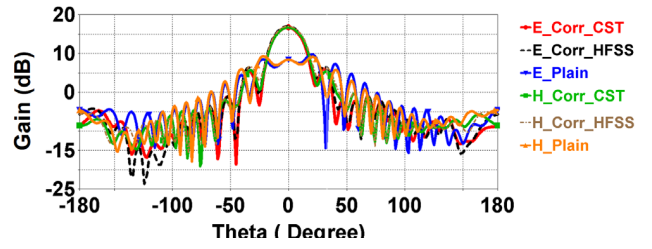
An important notice regarding the gain controlling of PLDC, that the gain is not affected by the corrugation period by itself, provided that it satisfies the propagation condition in (1). In fact, the corrugation duty cycles f controls the gain and the bandwidth of PLDC. The corrugation duty cycles f controls, basically, the phase constant of the modes according to (2) and (3). Fig.10 shows two cases for two different corrugation periods with the same duty cycle have identical gain. In other words, the corrugation duty cycle controls the propagation, the gain and the bandwidth of Quasi-Yagi antenna with PLDC lens. Radiation patterns of PLDC are compared to radiation patterns of an identical antenna with a plain substrate as shown in Fig. 11. PLDC has better performance over the plain one in terms of removing the effect of HOMs, especially, in high frequencies.

B. RAY COMBINER DIELECTRIC LENS

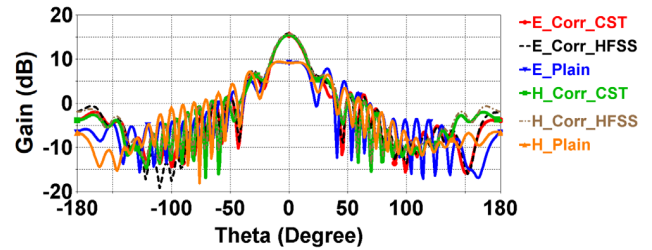
Ray Combiner Dielectric Lens (RCDL) is a dielectric lens with hybrid diffraction gratings that works as a spatial modulator for a propagating wave in DSW. It can be designed using



(a)



(b)



(c)

FIGURE 11. PLDC radiation pattern: (a) 30 GHz. (b) 32 GHz. (c) 34 GHz.

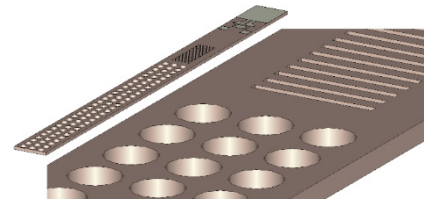


FIGURE 12. RCDL geometry as hybrid diffraction gratings.

the same methodology as the PLDC, except that, it contains two types of diffraction gratings, one and two-dimensional gratings as shown in Fig. 12. A sequence of $(L_{rs} \times w_{rs})$, d_r spaced rectangular slots is introduced perpendicular to the direction of the propagation to provide a smooth transition between the plain part of the DSW and the two-dimension circular holes' lattice of r_h radius with d_x and d_z sampling periods in x and z direction, respectively. all periods should satisfy the diffraction gratings phase condition in x and z -direction.

$$k_{z,m}^g = k_0 n_i \sin \theta_i + m \frac{2\pi}{d_z} \tag{4}$$

$$k_{x,m}^g = k_0 n_i \cos \theta_i + m \frac{2\pi}{d_x} \tag{5}$$

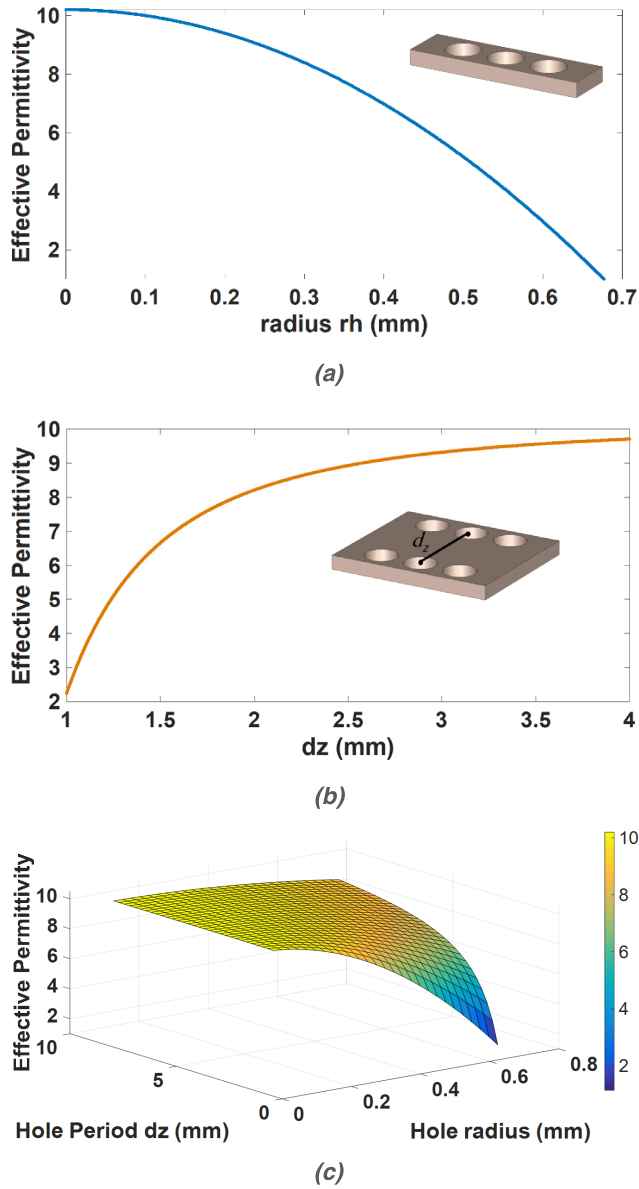


FIGURE 13. Effective dielectric constant of the substrate holed with cylindrical air-hole for different: (a) hole radius with fixed period of 1.25mm. (b) hole period with fixed radius of 0.5mm. (c) both of hole radius and period vary simultaneously.

$k_{x,m}^g$ and $k_{z,m}^g$ are related to each other by the dispersion equation as

$$k_{x,m}^g = \sqrt{(k_0 n_{eff})^2 - (k_{z,m}^g)^2} \quad (6)$$

When the magnitude of either $|k_{x,m}^g|$, $|k_{z,m}^g|$ increases due to phase mismatching between the incident wave and the grating surface, the phase constant $k_{x,m}^g$ changes from real to imaginary indicating an evanescent mode rather than propagating.

The major contribution to the RCDDL effective permittivity is due to the two-dimension circular holes' lattice and is given

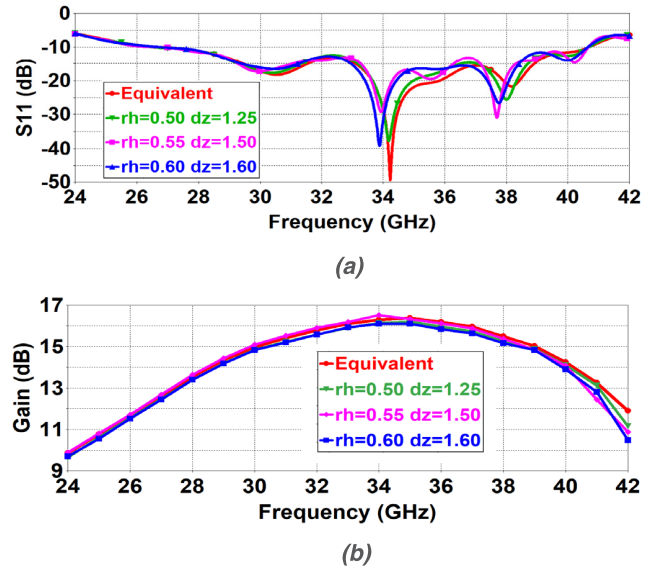


FIGURE 14. Comparison of simulated S11 and gain of Quasi Yagi antenna with RCDDL and equivalent models: (a) Return Loss. (b) Gain.

by

$$\epsilon_{eff} = \epsilon_r + \frac{\pi r_h^2}{d_x d_z} (1 - \epsilon_r) \quad (7)$$

$$N_h = \lfloor (a - 2c + s_x) / (2r_h + s_x) \rfloor \quad (8)$$

where r_h is the radius of the circular hole, N_h is the number of holes along x -axis and depends on some fabrication constraints like clearance margin (c) from substrate's edges and edge-to-edge spacing between adjacent holes (s_x), a is the substrate's width, and s_z is the edge-to-edge spacing between two adjacent holes along z -axis. For simplicity, N_h is set to be 3 and fixed for the simulation and fabrication processes, while r_h and s_z are varied during the simulation process. It should be noted that the period $d_x = (2r_h + s_x) = 1.254 \text{ mm}$ (fixed) and $d_z = (2r_h + s_z)$. An extraction model of the effective constant is illustrated in Fig. 13. To validate the equivalent effective dielectric constant model, the Quasi-Yagi antenna with RCDDL is simulated for three different combinations of hole radius and periodicity in z -direction selected from Fig. 13, to have the same effective dielectric constant calculated by (7) and are compared to a Quasi-Yagi antenna with a holed part replaced by a plain dielectric slab of the same thickness and equivalent dielectric constant. The simulation results depicted in Fig. 14 show that the performance of the proposed Quasi-Yagi antenna with RCDDL, for the selected combinations, agree well with the performance of the equivalent model. As the hole radius increases, the effective dielectric constant decreases and consequently, HOMs are forced to be evanescent according to (3) and (6). By increasing the hole radius, the antenna impedance matching is improved as shown in Fig. 15a, where only the fundamental mode is propagating. Though, Fig. 15b shows that the hole radius is inversely proportion to the antenna gain. The hole

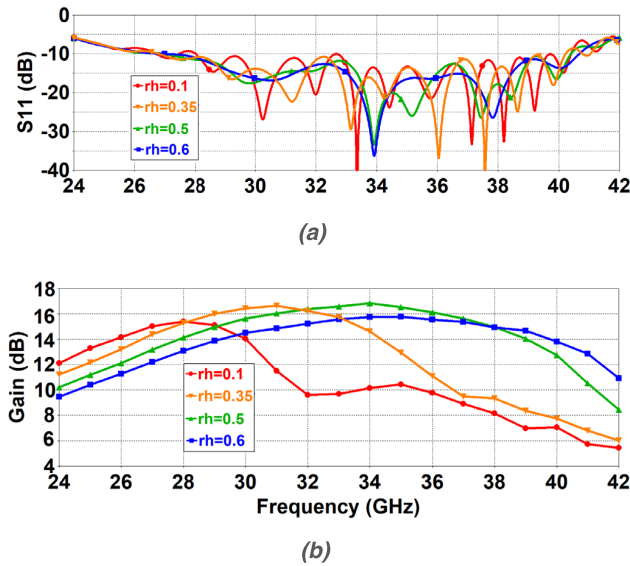


FIGURE 15. RCDL Performance variation with circular hole's radius: (a) Return Loss, (b) Gain.

radius should be optimized for a certain gain performance. In contrast, the increase of holing period leads to an effective dielectric constant increase. Therefore, HOMs would have real phase constant and start to interact destructively with the fundamental mode. this interaction deteriorates the antenna impedance matching as shown in Fig. 16a, while the antenna has a good impedance matching for small holing periods where only the fundamental mode is propagating. As the period becomes a significant fraction of effective wavelength, RCDL becomes an inhomogeneous medium. At hole period $d = \lambda_0 / \sqrt{\epsilon_{eff}}$, the maximum limit to preserve ZOD mode is reached. Then, RCDL looks to the incident wave as diffraction gratings. In this case, the wave is diffracted as $m = -1$ diffracted mode into the surrounding medium with a large portion is reflected to the antenna as shown in Fig. 16a. Subsequently, the gain sharply declines as shown in Fig. 16b.

For designing RCDL, we need to ensure that the incident wave is propagating as ZOD mode along the lens structure. According to (4) and (5), d_x and d_z periods should satisfy $d \ll \lambda_0 / \sqrt{\epsilon_{eff}}$.

The simulated E-plane (E), H-plane (H), and cross-polarization (XPol) radiation patterns of the RCDL Quasi-Yagi antenna are illustrated in Fig. 17, at 30 GHz, 34 GHz, and 38 GHz, respectively. The corresponding 3 dB beamwidth in E-plane and H-plane are around 32.6°, 28°, and 28°. Both E and H plane fields are symmetric with centered beam and almost have a similar 3 dB beamwidth. The simulation results show that RCDL highly improves the gain performance of the Quasi-Yagi antenna compared to the plain DSW lens and ranges between 14.7 to 15.8 dB. The side lobe level (SLL) is better than -15 dB for the band 30-34 GHz and better than -12 dB in the entire desired band. Moreover, the simulated cross-polarization level is about -29 dB within 3dB beamwidth in the entire 30-38 GHz band.

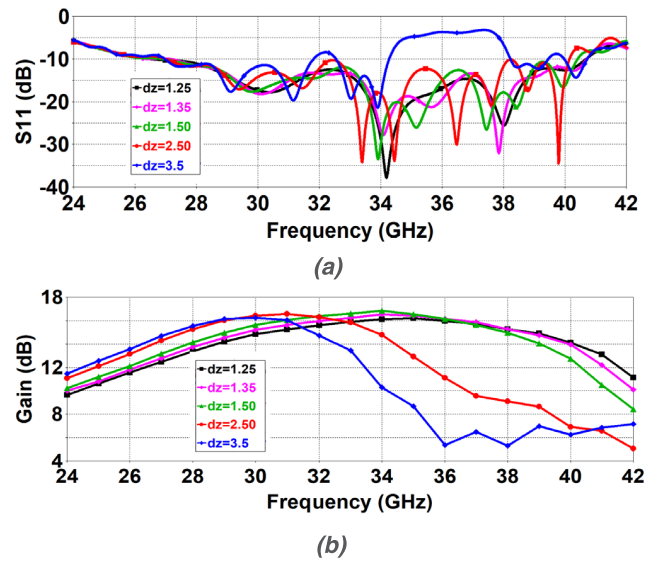


FIGURE 16. RCDL Performance variation with corrugation period: (a) Return Loss, (b) Gain.

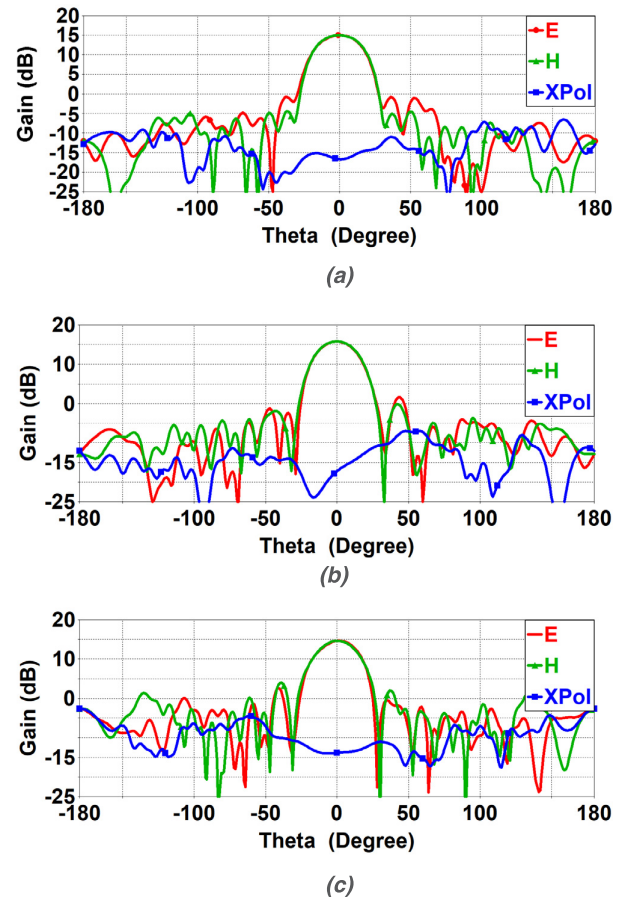


FIGURE 17. Simulation RCDL Quasi-Yagi antenna's radiation pattern: (a) 30 GHz. (b) 34 GHz. (c) 38 GHz.

It can be seen from Fig. 18 that the total efficiency of the proposed RCDL Quasi-Yagi antenna is about 90 % within 30-34 GHz and decreases almost linearly along with increasing of the attenuation due to the loss tangent of the dielectric.

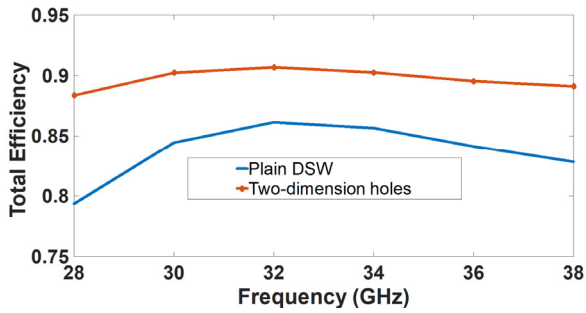


FIGURE 18. Simulation total efficiency of the Quasi-Yagi with a plain dielectric lens and with RCDL (Two-dimension holes).

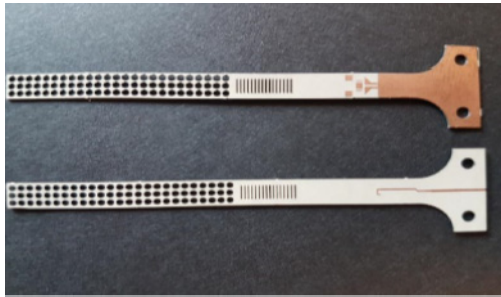


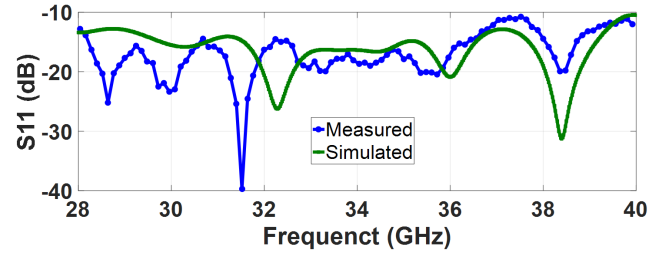
FIGURE 19. RCDL prototype.

Besides, the total efficiency of the RCDL Quasi-Yagi antenna is improved compared to that of the Quasi-Yagi with a plain DSW. Similarly, the simulation results show an aperture efficiency ranges from 95.6 % at 30 GHz to 54.7 % at 38 GHz.

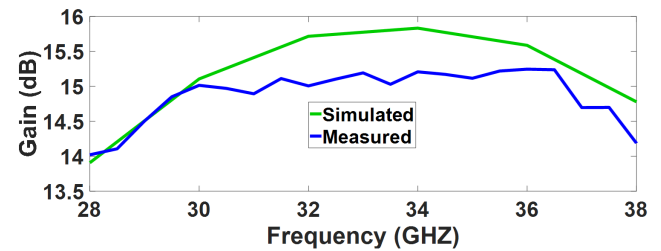
C. DESIGNING METHODOLOGY

The proposed Quasi-Yagi antenna with perturbed DSW based on gratings and effective medium theories can be designed according to the following brief and simple designing steps:

1. Determine the frequency bandwidth ($f_{min} - f_{max}$) assuming about 40% as initial guess FBW.
2. Select a substrate with a high dielectric constant to minimize the antenna size. The substrate thickness should allow good corrugation depth from mechanical prospective (avoid ceramic material), the thickness should be as minimum as possible to avoid cross-polarization, especially for higher mmWave frequencies.
3. On the top layer of the selected substrate, set the length of the following antenna parts to be:
 - a. Ground plane width of $\lambda 1.34_{eff}$ of the center frequency in the band.
 - b. One λ_{eff} driver for high directivity.
 - c. Use one (or more) multi-director of about $\lambda(0.25 \text{ to } 0.3)_{eff}$ width with about $\lambda(0.1 - 0.15)_{eff}$ spacing.
 - d. Keep around $\lambda 0.25_{eff}$ distance between driver and antenna ground plane.



(a)



(b)

FIGURE 20. RCDL Antenna Performance: (a) Return Loss. (b) Gain.

- e. Taper the driver to improve the antenna bandwidth performance.
 - f. Make a reasonable slot between the two sides of the driver to allow MS-to-SL transition. The slot's width is about $\lambda(0.1_{eff})$ and, generally, should be optimized to achieve a good antenna impedance matching.
4. On the bottom layer of the substrate, use a U-shape microstrip line of width corresponding to an impedance R_{in} , where R_{in} is the Quasi-Yagi array's input impedance measured at the center of the driver element. The dimensions of the balun should be optimized to counter the imaginary part of the input impedance ($R_{in} + jX_{in}$) and provide a good matching. This line is followed by section(s) of microstrip line to match the antenna to 50Ω port.
 5. Calculate the maximum effective dielectric constant that ensures single mode of operation using (3).
 6. Select proper air-hole radius and period using (7).
 7. Determine the number of holes along x-axis using (8)
 8. Set the total length of the antenna according to the required gain assuming an average aperture efficiency is 85%.

IV. EXPERIMENTAL RESULTS AND MANUFACTURING

To validate the proposed design methodology, one Quasi-Yagi antenna with perturbed substrate is fabricated and tested as shown in Fig. 19. The antenna is 4.5mm by 58.5 mm size.

The simulated and measured reflection coefficient of the antenna are shown in Fig. 20a. The antenna impedance matching is below -15 dB over a wide frequency band with some peaks around -10 dB at higher frequencies due to fabrication oversizing as shown in Fig. 21. The matching impedance bandwidth covers the band (24 – 40) GHz which

TABLE 2. Comparison of the proposed Quasi-Yagi Dielectric Lens antenna with other related works.

References	Excitation	Frequency, GHz	FBR, dB	XPol, dB	Gain, dBi	Efficiency %	Electrical Size mm ²	Yagi
[15]	MS-Patch	1.84-4.59	>10	-16	9	83 @ 3.5 GHz	0.58 λ ₀ × 1.1 λ ₀	Yes
[17]	MS-fed	22-26	20 @24 GHz	-16	10	90 @ 24 GHz	2.30 λ ₀ × 3.3 λ ₀	Yes
[18]	MS-to-SL	57-66	-	-15	11.7	-	1.84 λ ₀ × 2.0 λ ₀	Yes
[19]	Patch-fed	26-30	-	< -15	18.5	85 @ 28.5 GHz	11 λ ₀ × 13 λ ₀	No
This work	MS-to-SL	24-40	25 @30 GHz	< -20	15	90 @ 30 GHz	0.45 λ ₀ × 5.9 λ ₀	Yes

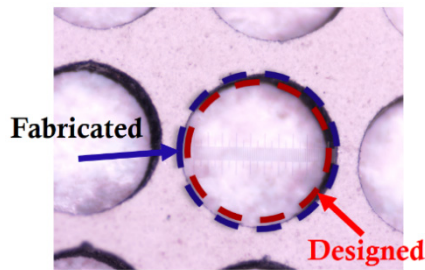


FIGURE 21. Fabrication oversizing.

is equivalent to 40% fractional bandwidth. The measured gain is about 14 to 15.2 dB over the band from 28 GHz to 38 GHz as shown in Fig. 20b. The radiation pattern at frequencies from 30 to 38 GHz are shown in Fig.15. A Cross-polarization level is better than -22 dB within the 3dB beamwidth for the entire frequency band. It can be seen from Fig. 20 and Fig. 22 that the simulation results agree well with the measured results. Measured gain flatness confirms the role of rectangular slots and circular hole subwavelength gratings. The proposed structure acts as a wide-bandpass filter by canceling the effect of HOM existed in the ordinary DSW. Measurement results show undesired SLL at 36 GHz and 38 GHz. This could be resulted by the oversizing of the antenna from the fabrication process. The circular hole, originally, is designed to be 1mm diameter, but the fabricated hole size is 1.1mm. The measured antenna aperture efficiency is compared to the simulated one as shown in Fig. 23. There are many reasons behind the difference between the measured and simulated results. The oversizing results in a slight gain reduction and SLL increase, especially, for higher frequencies compared to the simulation results of the proposed antenna. Furthermore, the loss tangent, according to the substrate’s datasheet, is 0.0023 at 10 GHz, but this value might be changed when the dielectric substrate is operated at 30-38 GHz and might result in additional losses. Besides, dielectric loss is inevitable decreases at higher frequencies. However, the measured results are quite encouraging taking into account the connector, cabling, and misalignment losses. The two-dimension circular holes’ lattice in DSW lens improves the gain and the bandwidth performance of

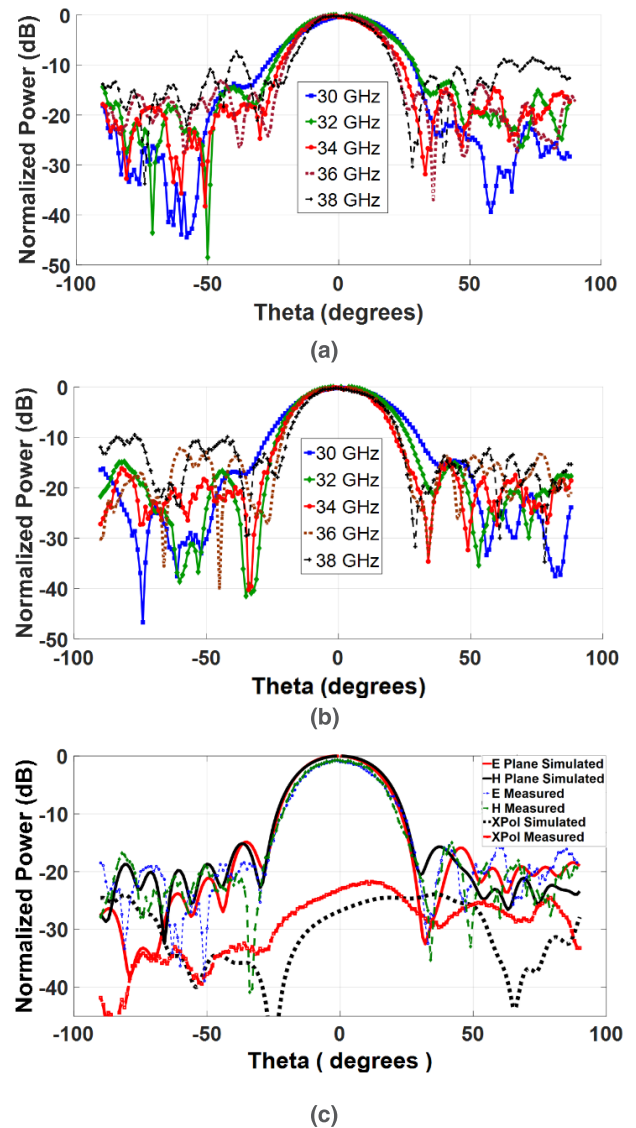


FIGURE 22. The radiation pattern of proposed RCGL: (a) Measured E plane. (b) Measured H plane. (c) Simulated and measured 34 GHz E, H and XPol.

the proposed antenna system compared to plain DSW lens. Furthermore, the proposed antenna is compared to some relevant planar mmWave antennas, such as Dielectric Lens

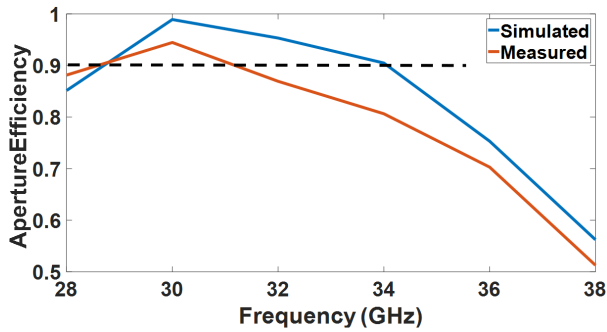


FIGURE 23. The aperture efficiency of the proposed Quasi-Yagi with RC DL.

antenna at 28.5 GHz, as well as, other Quasi-Yagi antennas at 3.2 GHz, 24 GHz, and 60 GHz. The performance of the proposed antenna is fairly better according to the reported results as summarized in Table 2.

V. CONCLUSION

A new millimeter-wave Quasi-Yagi antenna with a perturbed dielectric lens based on diffraction gratings and effective medium theories for gain enhancement, bandwidth broaden and higher order mode suppression is presented. The proposed design methodology is validated by designed, fabricated and measured antenna. The prototype experimental results show that the gain of the proposed antenna has been improved compared to the ordinary DSW lens. The proposed antenna exhibits a good impedance matching better than -15 dB in the band 24-40 GHz more than 17 GHz (40 % FBW). Measured cross-polarization level is better than -22 dB. The antenna measured gain ranges between 14 to 15.2 dB over the operating frequency band 30-38 GHz. This antenna can be considered as a competitive planar high gain antenna for 5G applications. It can be scaled to 60, 77, or 94GHz for 5G wireless point-to-point, point-to-multipoint backhaul communication systems, and automotive radar.

REFERENCES

- [1] T. S. Rappaport *et al.*, "Millimeter wave mobile communications for 5G cellular: It will work!" *IEEE Access*, vol. 1, pp. 335–349, May 2013.
- [2] Y. Hsu, T. Huang, H. Lin, and Y. Lin, "Dual-polarized quasi Yagi-Uda antennas with endfire radiation for millimeter-wave MIMO terminals," *IEEE Trans. Antennas Propag.*, vol. 65, no. 12, pp. 6282–6289, Dec. 2017. doi: [10.1109/TAP.2017.2734238](https://doi.org/10.1109/TAP.2017.2734238).
- [3] D. Liu, W. Hong, T. S. Rappaport, C. Luxey, and W. Hong, "What will 5G antennas and propagation be?" *IEEE Trans. Antennas Propag.*, vol. 65, no. 12, pp. 6205–6212, Dec. 2017. doi: [10.1109/TAP.2017.2774707](https://doi.org/10.1109/TAP.2017.2774707).
- [4] C. Jacob, K. Sabith, S. Prabhakaran, and N. Bhaskaran, "Planar printed Quasi-Yagi antenna—A study," *Int. J. Adv. Res. Elect., Electron. Instrum. Eng.*, vol. 4, no. 7, pp. 1–5, Jul. 2015. doi: [10.15662/ijareeie.2015.0407088.6562](https://doi.org/10.15662/ijareeie.2015.0407088.6562).
- [5] E. H. Mujammami and A. B. Sebak, "Design of a 30-GHz high gain Quasi-Yagi antenna," in *Proc. 32nd Gen. Assem. Sci. Symp. Int. Union Radio Sci. (URSI GASS)*, Montreal, QC, Canada, Aug. 2017, pp. 1–3. doi: [10.23919/URSIGASS.2017.8105181](https://doi.org/10.23919/URSIGASS.2017.8105181).
- [6] B.-Y. Park, M.-H. Jeong, and S.-O. Park, "A miniaturized microstrip-to-coplanar-strip transition loaded with artificial transmission lines and 2.4-GHz antenna application," *IEEE Antennas Wireless Propag. Lett.*, vol. 13, pp. 1486–1489, 2014. doi: [10.1109/LAWP.2014.2341552](https://doi.org/10.1109/LAWP.2014.2341552).
- [7] A. Hosseini and F. De Flaviis, "A CPW-fed single-layer printed Quasi-Yagi antenna for 60 GHz wireless communication systems," in *Proc. IEEE Antennas Propag. Soc. Int. Symp. (APSURSI)*, Memphis, TN, USA, Jul. 2014, pp. 103–104. doi: [10.1109/APS.2014.6904383](https://doi.org/10.1109/APS.2014.6904383).
- [8] H. K. Kan, R. B. Waterhouse, A. M. Abbosh, and M. E. Bialkowski, "Simple broadband planar CPW-fed Quasi-Yagi antenna," *IEEE Antennas Wireless Propag. Lett.*, vol. 6, no. , pp. 18–20, 2007. doi: [10.1109/LAWP.2006.890751](https://doi.org/10.1109/LAWP.2006.890751).
- [9] P. Wang and C. Cui, "Small-size CPW-fed Quasi-Yagi antenna with round-ended bow-tie CPW-to-slotline transition," in *Proc. IEEE Int. Symp. Radio-Freq. Integr. Technol. (RFIT)*, Taipei, Taiwan, Aug. 2016, pp. 1–3, doi: [10.1109/RFIT.2016.7578136](https://doi.org/10.1109/RFIT.2016.7578136).
- [10] J. Wu, Z. Zhao, Z. Nie, and Q.-H. Liu, "Bandwidth enhancement of a planar printed Quasi-Yagi antenna with size reduction," *IEEE Trans. Antennas Propag.*, vol. 62, no. 1, pp. 463–467, Jan. 2014. doi: [10.1109/TAP.2013.2287286](https://doi.org/10.1109/TAP.2013.2287286).
- [11] S. X. Ta, J. J. Han, H. Choo, and I. Park, "A wideband double dipole Quasi-Yagi antenna using a microstrip-slotline transition feed," in *Proc. IEEE Int. Workshop Antenna Technol. (iWAT)*, Tucson, AZ, USA, Mar. 2012, pp. 84–87. doi: [10.1109/IWAT.2012.6178404](https://doi.org/10.1109/IWAT.2012.6178404).
- [12] H.-D. Lu, L.-M. Si, and Y. Liu, "Compact planar microstrip-fed Quasi-Yagi antenna," *Electron. Lett.*, vol. 48, no. 3, pp. 140–141, Feb. 2012. doi: [10.1049/el.2011.3458](https://doi.org/10.1049/el.2011.3458).
- [13] Y. Lo, S. Wu, N. Liu, and J. Tarng, "A compact planar 60-GHz CPW-fed pattern reconfigurable Quasi-Yagi antenna," in *Proc. 12th Eur. Conf. Antennas Propag. (EuCAP)*, London, U.K., 2018, pp. 1–3. doi: [10.1049/cp.2018.0895](https://doi.org/10.1049/cp.2018.0895).
- [14] J. Tao, Q. Feng, and T. Liu, "Dual-wideband magnetoelectric dipole antenna with director loaded," *IEEE Antennas Wireless Propag. Lett.*, vol. 17, no. 10, pp. 1885–1889, Oct. 2018. doi: [10.1109/LAWP.2018.2869034](https://doi.org/10.1109/LAWP.2018.2869034).
- [15] H. Wang, S.-F. Liu, W.-T. Li, and X.-W. Shi, "Design of a wideband planar microstrip-fed Quasi-Yagi antenna," *Prog. Electromagn. Res. Lett.*, vol. 46, pp. 19–24, Apr. 2014. [Online]. Available: <http://www.jpier.org/PIERL/pier.php?volume=46>. doi: [10.2528/PIERL14031702](https://doi.org/10.2528/PIERL14031702).
- [16] M.-C. Tang, T. Shi, and R. W. Ziolkowski, "Flexible efficient Quasi-Yagi printed uniplanar antenna," *IEEE Trans. Antennas Propag.*, vol. 63, no. 12, pp. 5343–5350, Dec. 2015. doi: [10.1109/TAP.2015.2486807](https://doi.org/10.1109/TAP.2015.2486807).
- [17] R. A. Alhalabi and G. M. Rebeiz, "High-gain Yagi-Uda antennas for millimeter-wave switched-beam systems," *IEEE Trans. Antennas Propag.*, vol. 57, no. 11, pp. 3672–3676, Nov. 2009. doi: [10.1109/TAP.2009.2026666](https://doi.org/10.1109/TAP.2009.2026666).
- [18] L. Lu, K. Ma, F. Meng, and K. S. Yeo, "Design of a 60-GHz Quasi-Yagi antenna with novel ladder-like directors for gain and bandwidth enhancements," *IEEE Antennas Wireless Propag. Lett.*, vol. 15, pp. 682–685, 2016. doi: [10.1109/LAWP.2015.2469139](https://doi.org/10.1109/LAWP.2015.2469139).
- [19] L. Xue and V. Fusco, "Patch fed planar dielectric slab extended hemi-elliptical lens antenna," *IEEE Trans. Antennas Propag.*, vol. 56, no. 3, pp. 661–666, Mar. 2008. doi: [10.1109/TAP.2008.916974](https://doi.org/10.1109/TAP.2008.916974).
- [20] L. Xue and V. Fusco, "Patch-fed planar dielectric slab waveguide Luneburg lens," *Microw. Antennas Propag.*, vol. 2, no. 2, pp. 109–114, Mar. 2008. doi: [10.1049/iet-map:20070146](https://doi.org/10.1049/iet-map:20070146).
- [21] P. Yadav, S. Mukherjee, and A. Biswas, "Design of planar substrate integrated waveguide (SIW) phase shifter using air holes," *IEEE Applied Electromagnetics Conference (AEMC)*, Guwahati, India, Dec. 2015, pp. 1–2. doi: [10.1109/AEMC.2015.7509117](https://doi.org/10.1109/AEMC.2015.7509117).
- [22] Y. He, Z. Gao, D. Jia, W. Zhang, B. Du, and Z. N. Chen, "Dielectric metamaterial-based impedance-matched elements for broadband reflectarray," *IEEE Trans. Antennas Propag.*, vol. 65, no. 12, pp. 7019–7028, Dec. 2017. doi: [10.1109/TAP.2017.2763176](https://doi.org/10.1109/TAP.2017.2763176).
- [23] Y. Cai, Y. Zhang, Z. Qian, W. Cao, and L. Wang, "Design of compact air-vias-perforated SIW horn antenna with partially detached broad walls," *IEEE Trans. Antennas Propag.*, vol. 64, no. 6, pp. 2100–2107, Jun. 2016. doi: [10.1109/TAP.2016.2542841](https://doi.org/10.1109/TAP.2016.2542841).
- [24] Y. Li and K.-M. Luk, "Wideband perforated dense dielectric patch antenna array for millimeter-wave applications," *IEEE Trans. Antennas Propag.*, vol. 63, no. 8, pp. 3780–3786, Aug. 2015. doi: [10.1109/TAP.2015.2441118](https://doi.org/10.1109/TAP.2015.2441118).
- [25] C. A. Balanis, *Antenna Theory: Analysis and Design*, 3rd ed. Hoboken, NJ, USA: Wiley, 2005.
- [26] J. Huang and A. C. Densmore, "Microstrip Yagi array antenna for mobile satellite vehicle application," *IEEE Trans. Antennas Propag.*, vol. 39, no. 7, pp. 1024–1030, Jul. 1991. doi: [10.1109/8.86924](https://doi.org/10.1109/8.86924).

- [27] W. L. Stutzman and G. A. Thiele, *Antenna Theory and Design*, 3rd ed. Hoboken, NJ, USA: Wiley, 2013.
- [28] D. M. Pozar, *Microwave Engineering*, 4th ed. Hoboken, NJ, USA: Wiley, 2011.
- [29] R. Elliott, "On the theory of corrugated plane surfaces," *Antennas Propag., Trans. IRE Prof. Group on*, vol. 2, no. 2, pp. 71–81, Apr. 1954. doi: [10.1109/T-AP.1954.27975](https://doi.org/10.1109/T-AP.1954.27975).
- [30] C. Palmer and E. Loewen, *Diffraction Grating Handbook*, 7th ed. Rochester, NY, USA: Newport, 2014.
- [31] E. G. Loewen and E. Popov, *Diffraction Gratings and Applications*. 7th ed. New York, NY, USA: Marcel Dekker, 1997.
- [32] E. Popov, *Gratings: Theory and Numeric Applications*, 1st ed. Marseille Cedex, France: Institut Fresnel, Univ. d'Aix-Marseille, CNRS Faculté Saint Jérôme, 2012.



ESSA H. MUJAMMAMI (GS'18) received the B.Sc. and M.Sc. degrees in electrical engineering from King Saud University, Riyadh, Saudi Arabia, in 2001 and 2006, respectively. He is currently pursuing the Ph.D. degree in electrical and computer engineering with Concordia University, Montreal, QC, Canada. He was an Electrical Engineer with the General Directorate of Communication in the Ministry of Interior (MOI), Saudi Arabia, from 2008 to 2010, and then the Director of ICT at MOI, from 2010 to 2014. His research interests include millimeter-wave, microwave components, and antennas.



ABDELRAZIK B. SEBAK (LF'18) received the B.Sc. degree (Hons.) in electrical engineering from Cairo University, Cairo, Egypt, in 1976, the B.Sc. degree in applied mathematics from Ein Shams University, Cairo, in 1978, and the M.Eng. and Ph.D. degrees in electrical engineering from the University of Manitoba, Winnipeg, MB, Canada, in 1982 and 1984, respectively. From 1984 to 1986, he was with Canadian Marconi Company, involving in the design of microstrip phased array antennas. From 1987 to 2002, he was a Professor with the Department of Electronics and Communication Engineering, University of Manitoba. He is currently a Professor with the Department of Electrical and Computer Engineering, Concordia University, Montreal, QC, Canada. His research interests include phased array antennas, millimeter-wave antennas and imaging, computational electromagnetics, and interaction of EM waves with engineered materials and bioelectromagnetics. He is a member of the Canadian National Committee of the International Union of Radio Science Commission B. He was a recipient of the 1994 Rh Award for Outstanding Contributions to Scholarship and Research, the 1996 Faculty of Engineering Superior, and the 2000 and 1992 University of Manitoba Merit Award for Outstanding Teaching and Research. He has served as the Chair for the IEEE Canada Awards and Recognition Committee, from 2002 to 2004, and as a Technical Program Chair for the 2002 IEEE CCECE Conference and the 2006 URSI ANTEMS symposium. He is a Technical Program Co-Chair of the 2015 IEEE ICUWB Conference.

...